Chinese Chemical Letters 36 (2025) 110066

Contents lists available at ScienceDirect

Chinese Chemical Letters

journal homepage: www.elsevier.com/locate/cclet

Face-to-face π-π interactions and electron communication boosting efficient reverse intersystem crossing in through-space charge transfer molecules

Manlin Lu[a,1], Sheng Liao[a,1], Jiayu Li[a], Zidong Yu[a], Ningjiu Zhao[c], Zuoti Xie[d], Shunli Chen[a,*], Li Dang[a,b,*], Ming-De Li[a,b,*]

[a] College of Chemistry and Chemical Engineering, Key (Guangdong-Hong Kong Joint) Laboratory for Preparation and Application of Ordered Structural Materials of Guangdong Province, Shantou University, Shantou 515063, China
[b] Chemistry and Chemical Engineering Guangdong Laboratory, Shantou 515031, China
[c] Songshan Lake Materials Laboratory, Dongguan 523808, China
[d] Department of Materials Science and Engineering, MATEC, Guangdong Technion-Israel Institute of Technology, Shantou 515063, China

ARTICLE INFO

Article history:
Received 13 April 2024
Revised 26 May 2024
Accepted 27 May 2024
Available online 28 May 2024

Keywords:
Through-space charge transfer
Reverse intersystem crossing
Thermally activated delayed fluorescence
Transient absorption
Through-bond charge transfer

ABSTRACT

The excited state dynamics and critically regulated factors of reverse intersystem crossing (RISC) in through-space charge transfer (TSCT) molecules have received insufficient attention. Here, five molecules of through space/bond charge transfer inducing thermally activated delayed fluorescence (TADF) are prepared, and their excited state charge transfer processes are studied by ultrafast transient absorption and theoretical calculations. DM-Z has a larger ΔE_{ST}, leading to a longer lifetime of intersystem crossing (ISC), resulting in the lowest photoluminescence quantum yield (PLQY). Oppositely, ISC and RISC are demonstrated to take place with shorter lifetimes for TSCT molecules. The face-to-face π-π stacking interactions and electron communication enable DM-B and DM-BX to have an efficient RISC, increasing the weight coefficient of RISC from 1.7% (DM-X) to close to 50% (DM-B and DM-BX) in the solvents, which make DM-BX and DM-B to have a high PLQY. However, partial local excitation in the donor center is observed and the charge transfer is decreased for DM-G and DM-X. The triplet excited state (DM-G) or singlet excited state (DM-X) mainly undergoes inactivation through a non-radiative relaxation process, resulting in less RISC and low PLQY. This work provides theoretical hints to enhance the RISC process in the TADF materials.

As the third-generation organic light-emitting diode (OLED) materials, thermally activated delayed fluorescence (TADF) molecules can reach up to 100% exciton utilization without using noble metal complexes, thus attracting widespread attention in recent years [1-4]. High-performance TADF molecules have sufficiently small singlet-triplet energy gaps ($\Delta E_{ST} < 0.1$ eV) so that the triplet exciton can be converted into singlet exciton by the thermally assisted reverse intersystem crossing (RISC) process [5-9]. Molecules with donor-acceptor (D-A) features could have separate electron distribution at HOMO and LUMO and relatively small ΔE_{ST} [10-14] due to the charge transfer (CT), facilitating the intersystem crossing (ISC) and RISC. Despite there is substantial effort to understand the mechanism of RISC in TADF emitters, relatively little attention has been given to the role of excited state dynamics and critical regulated factors in this process [15].

There are two different types of CT, through-bond CT (TBCT) and through-space CT (TSCT) in TADF molecules [16]. In recent years, TSCT has been widely developed to construct TADF molecules in OLED materials to obtain high luminescent efficiency [11,17-36]. Triphenylamine (TPA) and triazine have been used as excellent electron D-A pairs due to their multi-ring conjugated structure, as well as strong hole transport ability [37]. Therefore, X. Tang and coworkers chose rigid modified TPA and 2,4,6-triphenyl-1,3,5-triazine as the donor and acceptor units to design a series of TSCT molecules (DM-B, DM-Bm, DM-G, DM-X) and a TBCT molecule (DM-Z) [38]. It demonstrated that the higher photoluminescent quantum yield (PLQY) could be achieved in space-confined charge-transfer emitters (DM-B (96%), DM-Bm (92%), and DM-G (88%)) doped in DPEPO film, respectively. In comparison, less rigid emitters (DM-X) reach a substantially lower PLQY of 32% doped in DPEPO film, and then the TBCT emitter DM-Z displays the lowest

* Corresponding authors.
E-mail addresses: chenxl@stu.edu.cn (S. Chen), ldang@stu.edu.cn (L. Dang), mdli@stu.edu.cn (M.-D. Li).
[1] These authors contributed equally to this work.

https://doi.org/10.1016/j.cclet.2024.110066
1001-8417/

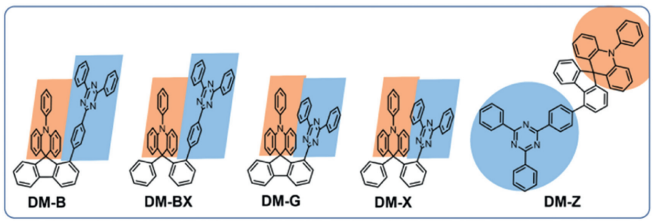

Scheme 1. Chemical structures of the TADF molecules studied.

PLQY of 23% doped in DPEPO film. The photophysical process and the internally regulated factors on ISC and RISC of these TSCT and TBCT molecules are still unclear, greatly hindering the design and development of TADF materials [39].

Here, we synthesized four TSCT molecules (DM-B, DM-BX, DM-G, DM-X) and one TBCT molecule (DM-Z) (Scheme 1 and Fig. S1 in Supporting information), in which a less rigid bridge emitter DM-BX was designed as the control experiment of DM-B to investigate how the rigidity affects PLQY. The excited-state dynamics, critically regulated factors of ISC/RISC, and luminescent mechanism of these molecules were explored by using ultrafast femtosecond to nanosecond transient absorption (fs-TA, ns-TA) spectra and theoretical calculations [40-42]. The theoretical calculations were carried out using the Gaussian 16 software packages [43]. The distributions of holes and electrons, interaction region indicator (IRI) analysis, and CT matrix analysis were performed by excited state calculations with time-dependent density functional theory (TDDFT) methods.

Fig. S2 (Supporting information) shows the normalized UV–vis absorption and emission spectra of DM-B, DM-BX, DM-G, DM-X, and DM-Z dissolved in five different polar solvents. In these solvents, the low-intensity tail absorption stretching from 350 nm to 450 nm is observed for DM-B, DM-BX, DM-G and DM-X, indicating a weak intramolecular CT taking place at ground state. However, the extended tail absorption is absent for DM-Z, indicating intramolecular CT may not occur in the ground state. These results indicate that when D-A are close to each other, which results in significant orbital space coupling, the CT process of D-A molecules will occur at the ground state [44]. Differently, the fluorescence emission peaks of all emitters show a red shift with a large Stocks shift with the increase of solvent polarity from toluene to DMF (Fig. S2). Furthermore, the absolute PLQY of TSCT and TBCT molecules were tested in DCM, DMF and toluene solvents. As illustrated in Fig. S2, DM-B exhibits the highest PLQY of 56.1%, followed by DM-BX (45.4%), DM-G (18.6%) and DM-X (8.7%) in polar solvent DCM. The PLQY with rigid bridge molecules is obviously larger than the one with corresponding flexible bridge molecules (DM-B > DM-BX, DM-G > DM-X). In contrast, the PLQY of all molecules decreased to a certain extent in the high polar solvent (DMF). However, DM-BX has the highest PLQY of 44.9%, followed by DM-B (22.5%), DM-G (3.1%), DM-X (1.8%) and DM-Z (4.2%) have the low PLQY in toluene, indicating that localized excitation rather than TSCT or TBCT are dominant in toluene which is not favorable to RISC, leading to the low PLQY. Importantly, no matter whether in a polar solvent or high polar solvent, molecules containing benzene ring spacer between acceptor and bridge have better PLQY (DM-B > DM-G, DM-BX > DM-X) and TBCT molecule DM-Z displays the lowest PLQY.

All of these emitters display the CT process after excitation based on fluorescence emission spectra, and the absolute PLQY has a certain regularity. Therefore, it is necessary to explore their excited state evolution processes, luminescent mechanism and the key factors affecting their luminescent properties from the perspective of excited state dynamics. To trace the excited-state evolution of these emitters and unveil the CT process, fs-TA and ns-TA experiments are performed in different solvents (DCM and DMF) with different polarity upon 400 nm (for TSCT molecules) and 320 nm (for TBCT molecule) excitation (Fig. 1 and Figs. S3-S9 in Supporting information).

Fig. 1a shows that the excited state absorption (ESA) peak of DM-B is quite broad, with three obvious excited-state evolution processes. At the beginning of 0.65 ps, two primary ESA peaks at 662 and 750 nm rise quickly. Because the ESA peak at 750 nm is the characteristic peak of TPA cation radical [45], this process can be attributed to the CT process that generates an excited charge separation (CS) state. After that, the fs-TA spectra change significantly from 0.65 ps to 380 ps. The ESA peak at 750 nm continues to rise, and the ESA peak at 662 nm redshifts gradually and becomes a shoulder peak. The redshift of the peak at 662 nm indicates that this process may be accompanied by the solvation relaxation. At the end of the delay time, all ESA peaks decline slowly. It is worth noting that a negative peak at 550 nm is gradually generated after 3.86 ns, which is consistent with the fluorescence emission peak (around 550 nm) in DCM solvent. Notably, the negative peak at 550 nm is absent when the solvent is changed into polar solvent DMF (Fig. 1a). As seen from fs-TA spectra, the ESA peak with a strong signal still exists after 7.21 ns. Hence, ns-TA is used to track the complete excited-state evolution processes of DM-B (Fig. 1b). Like fs-TA, the broad ESA band of DM-B is also detected in ns-TA spectra after 400 nm excitation, and the prominent ESA peak is located at 691 nm. The ESA peak at 691 nm rises before 1.32 ns, then decays to about zero at 1.05 μs. According to the kinetic decay curve of ns-TA (Fig. 1c), the ESA peak at 691 nm decays faster under an oxygen atmosphere. The specific lifetime values are obtained by two exponential functions fitting its kinetic decay curve (Fig. S10 in Supporting information). In the nitrogen atmosphere, τ_1 and τ_2 are 33.1 and 201 ns, respectively. In contrast, in the oxygen atmosphere, τ_1 and τ_2 reduce to 2.5 and 29 ns (Fig. S11 in Supporting information), respectively, indicating that the ESA peaks at 691 nm can be assigned to a triplet state species. In addition, we also explored DM-BX, DM-G, and DM-X by fs-TA and ns-TA spectra. The results indicate that all of them have similar excited-state evolution processes to DM-B (Figs. S3-S9), except for the different lifetimes of excited-state dynamics.

Notably, the ESA peaks at 600–850 nm of ns-TA spectra were always dominant from beginning to end for TSCT molecules in DCM, while ESA peaks at 520–540 nm were absent. According to the oxygen quenching experiment, ESA peaks at 600–850 nm belong to the triplet excited state. Previous studies found that transient absorption peaks near 520–540 nm are thought to be the triplet excited state in the toluene solvent [38]. To confirm this peak, fs-TA and ns-TA experiments were also conducted on TSCT molecules in a toluene solvent (Figs. S12-S15 in Supporting information). According to the ns-TA spectra of DM-B in toluene, the ESA peak at 674 nm decays rapidly, while the ESA peak at 551 nm decays slowly, and no isosbestic points can be observed. The ESA peak observed at 551 nm is consistent with the original report [38]. According to previous work, this ESA peak at 551 nm could be assigned to a local triplet excited state (T_1) for DM-B, which is consistent with the theoretical calculations of T_1 for DM-B [38]. For DM-BX, DM-G, and DM-X, the ESA peak at 551 nm can not be observed while only a broad peak at 600–850 nm slowly decays to zero. This is also consistent with the theoretical calculations of excited states, in which a CT triplet excited state can be obtained for DM-G and DM-X.

According to the transient absorption evolution processes and the known properties of the excited state for TADF materials, the excited state evolution processes of TSCT molecules (DM-B, DM-BX, DM-G, and DM-X) are divided into five steps. τ_1, τ_2 and τ_3 were fitted according to fs-TA spectra (Fig. S16 in Supporting in-

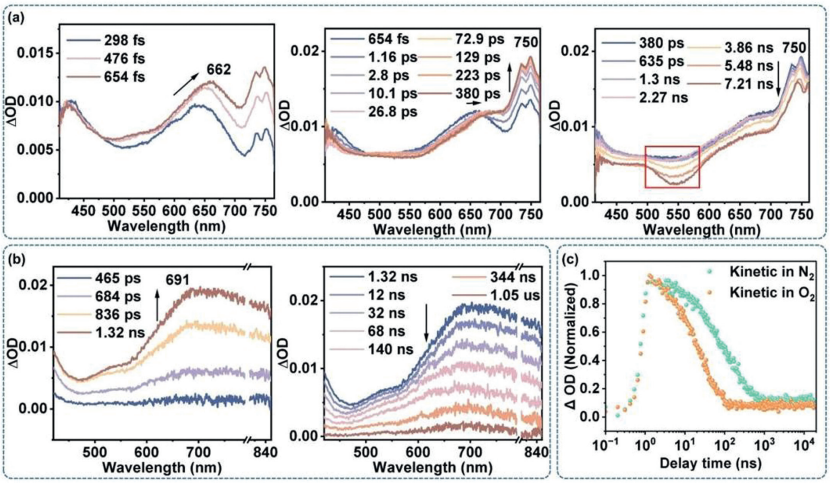

Fig. 1. Transient absorption spectra measurements of DM-B in DCM solvent after 400 nm excitation. (a) fs-TA spectra of DM-B recorded at different delay times; (b) ns-TA spectra of DM-B recorded at different delay times; (c) ns-TA spectra decay curve at 691 nm of DM-B purged by N_2 and O_2.

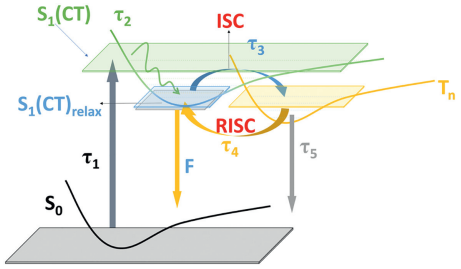

Scheme 2. Schematic diagram illustrating the Jablonski energy levels of DM-B, DM-BX, DM-G and DM-X.

formation), the last two lifetimes (τ_4 and τ_5) are the decay lifetimes fitted according to ns-TA spectra (Fig. S10), and the detailed data are summarized in Table S2 (Supporting information). All the TSCT molecules will undergo the CT process after excitation. Therefore, the excited state dynamics of these molecules exhibit a solvent-polar dependence. Table S2 shows that the lifetimes of DM-B, DM-BX, DM-G and DM-X are obviously different, the most of lifetimes of DM-B, DM-BX, DM-G and DM-X in DMF solvent are longer than that obtained in DCM solvent. The excited-state evolution processes of TSCT molecules can be explained as the following Scheme 2. τ_1 is the growing lifetime of ESA peak at 750 nm, which is attributed to the formation process of TPA cation radical, that is, the population of S_1 with CS feature (denoted as $S_1(CS)$). τ_2 is described as the lifetime of $S_1(CS)$. The lifetime of τ_2 for DM-G is the longest (close to 20 ps), followed by DM-B, DM-BX, and DM-X (within 5 ps). During the process from the vertical S_1 state to the adiabatic S_1 state, the molecular structure of DM-G changes the most. As expected, it requires more time to go through the structural relaxation process (the detail is described in theoretical calculations in Supporting information). Therefore, the second lifetime should be attributed to the structural relaxation to convert into the $S_1(CS)_{relax}$ [46]. τ_3 is depicted as the lifetime of ISC for $S_1(CS)_{relax}$. For all TSCT molecules, τ_3 obtained in the DCM solution is smaller than that obtained in the DMF solution (Table S2). This is because $S_1(CS)_{relax}$ species has a high-degree CS character, whereas molecules in the CS state are more stable in the polar solvent DMF. Dipole-dipole interaction makes the $S_1(CS)_{relax}$ likely to stay in the CS state and then return to the ground state by the nonradiative decay process, rather than rapidly convert to other excited state species (triplet state) [47]. Therefore, TSCT molecules are prone to undergo the ISC process in the low polar solvent DCM, whereas the ISC process takes a longer time in the high polar solvent DMF, which is also consistent with the experimental results of PLQY: the PLQY of TSCT molecules decreases with the increase of solvent polarity. Ns-TA spectra results reveal that all TSCT emitters will generate a long-lived triplet excited state species after 400 nm excitation. Therefore, $S_1(CS)_{relax}$ will be converted into the triplet excited state by the ISC process as well. The last two lifetimes (τ_4 and τ_5) are possibly attributed to the decay of the triplet excited states, which are fitted according to the ns-TA spectra (Fig. S10). τ_4 is the lifetime of RISC process of the triplet state. According to the theoretical calculation in the following section, the ΔE_{ST} of these TSCT emitters is relatively small, so the RISC process may occur in all of them. Unprecedentedly, the weighted amplitude of τ_4 in DM-B and DM-BX is close to 50% (in DCM and DMF solvent). Therefore, these molecules are more likely to undergo the RISC process, followed by DM-G.

Notably, only the sequential reaction will have a clear isosbestic point, which will show the growth and decay of the different excited states, while for a parallel reaction, the isosbestic points usually cannot be observed. In the fs-TA spectra, the ISC growing process of DM-B, DM-BX, DM-G and DM-X is observed in the second process of Fig. 1a and Figs. S3a-S9a, the clear isosbestic points can be observed. However the repopulation of the singlet state *via* RISC cannot be observed in the ns-TA spectra, this is because the S_1 and T_1 of TSCT molecules are both CS states. Generally speaking, the CS states usually have a broad transient absorption, therefore, the positions of their absorption peaks may be similar or even overlapping. In addition, there is also some competition from other processes accompanied by the RISC process, so we do not finally observe the appearance of isosbestic points in the ns-TA. For DM-X, although the k_{RISC} (lifetime) of DM-X is the fastest among other TSCT molecules, the weighted amplitude of RISC (τ_4) for DM-X is the smallest among these TSCT molecules, so it is difficult for DM-X to undergo the RISC process. Furthermore, we combined the average lifetime of decay kinetic processes (τ_4 and τ_5) of ns-TA (Fig. S10d) with the fluorescence lifetime measured by time-resolved fluorescence spectra (Fig. S10c) to calculate the radiative transition rate constant and non-radiative transition rate constant. Compared with other TSCT molecules, the lifetimes of DM-X obtained by ns-TA and time-resolved fluorescence measurements are similar, which suggests that there may be no ISC process in DM-X, and most of the energy is dissipated by fluorescence emission or consumed by non-radiative transition processes. These results are con-

Table 1
Summarized lifetimes of ns-TA and time-resolved fluorescence of these molecules in DCM solvent.

Dye	M (g/mol)	λ_{ex} (nm)[a]	λ_{em} (nm)[b]	Φ_F (%)	τ (ns)[c]	τ_F (ns)[d]	k_r (s^{-1}) [e]	k_{nr} (s^{-1}) [e]
DM-B	714.87	400	558	56.1	188	1456	6.9E+05	4.6E+06
DM-BX	716.87	400	555	45.4	398	1299	7.7E+05	1.7E+06
DM-G	638.77	400	565	18.6	138	1401	7.1E+05	6.5E+06
DM-X	640.79	400	540	8.7	21	18.5	5.4E+07	/
DM-Z	714.87	320	559	1.1	1800	108	9.2E+06	/

[a] Excitation wavelength,
[b] emission wavelength,
[c] lifetime of ns-TA,
[d] lifetime of TRPL
[e] Radiative and non-radiative rates.

sistent with the fact that DM-X has the smallest QLQY (Table S1 in Supporting information). This reveals that the RISC process greatly contributes to the PLQY of these four TSCT molecules.

Interestingly, a negative peak at 550 nm is gradually generated after 3.86 ns in the fs-TA spectra (Fig. 1a) of DM-B (in the same time range of RISC), indicating that triplet state species are changed into singlet excited states by the RISC process. τ_5 is attributed to the relaxation process of the triplet state. As the polarity of the solvent increases, τ_5 of TSCT molecules tends to be prolonged, indicating that the triplet state also has a character of the CS state. Therefore, the triplet state is relatively stable and requires a longer time for non-radiative processes in the polar solvent DMF, such as charge recombination, to return to the ground state. To further demonstrate the TSCT process of the excited states, femtosecond time-resolved up-conversion fluorescence (fs-TRUCF) spectroscopy with 120 fs time resolution [24] is used to track the transient fluorescence spectra of DM-B and DM-X (Fig. S17 in Supporting information). Within 0.15 ps to 3.36 ps, the fs-TRUCF spectra of DM-B are redshifted from 510 nm to 550 nm. In comparison, DM-X is redshifted from 550 nm to 560 nm, demonstrating that both DM-B and DM-X can undergo the TSCT process in the excited state, and DM-B has a larger CT degree than DM-X and therefore has a larger spectral redshift. In addition, to correctly obtain the lifetime of fluorescence for these TADF molecules, time-resolved fluorescence measurements are carried out on TSCT molecules and TSBT molecules in DCM solvent, which only can detect the bright singlet excited states (irradiative process). Time-resolved fluorescence spectra decay curve at 550 nm can be fitted by two exponential functions for DM-B, DM-BX and DM-G, while one exponential function for DM-X (Fig. S10). As for DM-B, DM-BX and DM-G, the short lifetimes may be related to the normal fluorescence and the long lifetimes could be related to TADF emission. While for DM-X, only a short lifetime (18.5 ns) could be obtained, which is related to the normal fluorescence. This indicates that DM-X will not undergo RISC process, which is consistent with ns-TA results. However, when transient absorption is used to trace the dynamics of these TSCT molecules, both the bright and dark states (irradiative process and non-irradiative process) could be detected by fs-TA and ns-TA. Therefore, the average fluorescence lifetime fitted from the time-resolved fluorescence spectra can be combined with the average lifetime fitted from the ns-TA decay process to calculate the irradiation and non-irradiation rate constants (Table 1), *e.g.*, DM-B, the non-radiative transition rate constant ($k_{nr} = 4.6 \times 10^6$ s^{-1}) of DM-B is about one order of magnitude higher than the radiative transition rate constant ($k_r = 6.9 \times 10^5$ s^{-1}). It must be noted that the non-irradiated process is faster than that of the irradiated process. Therefore, we cannot simply assign the lifetimes of ns-TA for these TSCT molecules in the solution phase to the prompt (fluorescence) and delayed (RISC) emission, respectively. In fact, the first lifetime (33 ns) obtained from ns-TA for DM-B in DCM solvent is obviously shorter than that (54 ns) obtained from time-resolved fluorescence measurement. As proposed, the DM-B will undergo the ISC process with a lifetime of 81.6 ps, and then the most of triplet states will undergo the RISC process to return to the singlet excited state and a small partial triplet states will undergo the non-irradiative process to return to the ground states. Furthermore, the average lifetimes obtained from ns-TA for DM-B, DM-BX and DM-G were dramatically shortened when we performed oxygen-replacing nitrogen-purged experiments (Figs. S10 and S11), this revealed that transient states involved in the ns-TA experiments have triplet state nature. While for DM-X, the average lifetimes obtained from ns-TA were slightly shortened when we performed oxygen replacing nitrogen purged experiments (Figs. S10 and S11), this revealed that transient states involved in the ns-TA experiments may be the singlet state. Therefore, the RISC process is not detected by ns-TA for DM-X in DCM, which explains that DM-X has the lowest PLQY value among these TSCT molecules.

Turning to the TBCT emitter DM-Z, we also employed fs-TA and ns-TA to probe its excited-state evolution processes. In a polar solvent DCM, three ESA peaks of 472, 653, and 750 nm are observed in the fs-TA spectra of DM-Z (Fig. 2a). Within the first 0.82 ps, all ESA peaks rise dramatically, the observation of the ESA peak at 750 nm indicates that the ICT occurs and TPA cation radical is formed during this process. Then, the ESA peak at 472 nm gradually decreases, blueshifts to 462 nm, and the ESA peak at 653 nm red-shifts to 660 nm. Finally, all ESA peaks continue to fall, and the ESA peak at 660 nm redshifts to 665 nm. Because there is a strong and broad ESA signal at 7.2 ns, ns-TA is also used to explore the excited-state evolution process. As shown in Fig. 2b, two prominent ESA peaks at 443 and 685 nm rise rapidly within 1.21 ns. Then, from 1.21 ns to 99.3 ns, the ESA peaks at 443 and 685 nm gradually decrease. At the same time, the ESA peak at 554 nm starts to rise. Two isosbestic points are observed at 484 and 615 nm, indicating the reaction conversion process between two transient species. After 99.3 ns, all ESA signals decrease slowly. To verify whether the new ESA peak at 554 nm can be assigned to the triplet state, oxygen quenching experiments have been conducted. As demonstrated in Fig. 2c, the kinetics of the ESA peak at 554 nm in the oxygen atmosphere decay faster than that in the nitrogen atmosphere. The specific lifetime data are obtained by two exponential functions fitting (Figs. S18 and S19 in Supporting information). The lifetimes τ_1 and τ_2 are 89 ns and 1.88 us in the nitrogen atmosphere. In contrast, the values of τ_1 and τ_2 are almost reduced by an order of magnitude to 11.6 ns and 177 ns in the oxygen atmosphere. This reveals that the ESA peak at 554 nm is attributed to the triplet state of DM-Z. Therefore, the conversion process from the ESA peaks at 443 and 685 nm to the ESA peak at 554 nm should be attributed to the ISC process. Notably, we can clearly observe the decay of ^{1}CT and the population of triplet state for DM-Z by ns-TA in DCM solvent. The possible reason is that the triplet state of DM-Z in DCM solvent has a local excitation (^{3}LE) property rather than a CT property. Therefore, the absorption peak of the triplet state for DM-Z in DCM appears at 554 nm while the absorption peak of the triplet CT state (^{3}CT) for TSCT molecules is

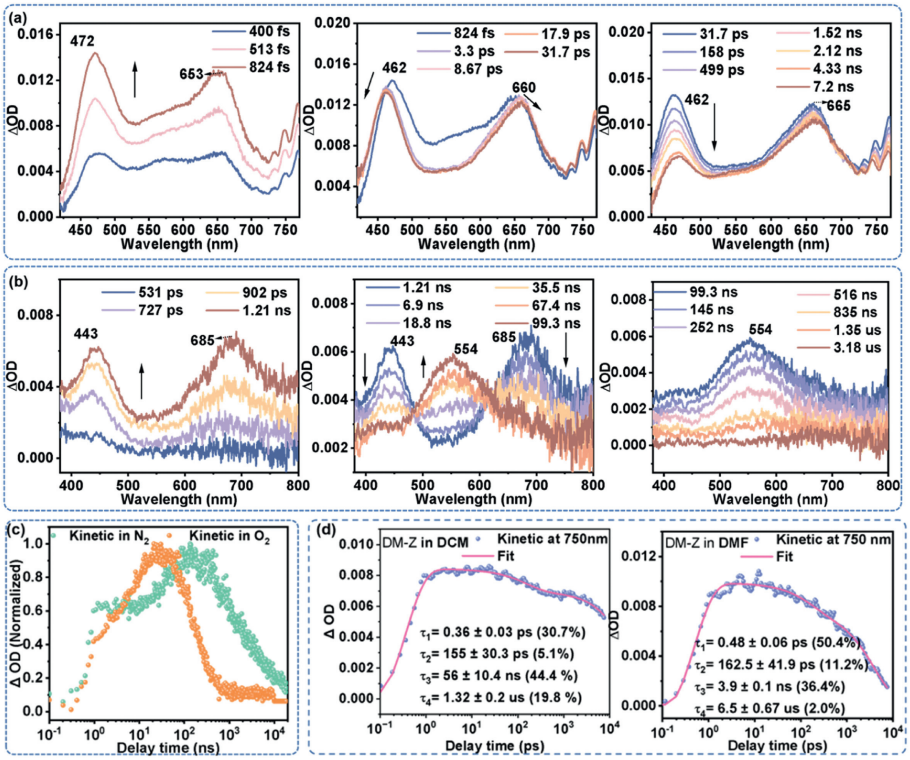

Fig. 2. Transient absorption spectra measurements of DM-Z. (a) fs-TA spectra of DM-Z recorded in DCM solution after 320 nm excitation. (b) ns-TA spectra of DM-Z recorded in DCM solution after 320 nm excitation. (c) ns-TA spectra decay curve at 554 nm of DM-Z in N_2 and O_2 purged conditions. (d) fs-TA spectra decay curve at 750 nm of DM-Z in DCM and DMF solutions, respectively.

Table 2
Summarized lifetimes and weighted amplitudes associated with exponential decay fitting of DM-Z in different polarity solvents.

Sample	τ_1 (ps)	τ_2 (ps)	τ_3 (ns)	τ_4 (μs)
DCM	0.35 (13.5%)	155 (2.3%)	89 (67.1%)	1.88 (26.8%)
DMF	0.48 (50.4%)	141 (10.3%)	3.9 (87.3%)	6.48 (12%)

located at 670–690 nm. Interestingly, when going from DCM solvent to a higher polarity solvent (DMF), environment-sensitive ^{3}CT gets lower than the ^{3}LE, thus ^{3}LE of DM-Z cannot be observed in DMF solvent (Fig. S20 in Supporting information). However, when DM-Z is dissolved in toluene with lower polarity (Fig. S21 in Supporting information), the ISC conversion process from singlet excited state to triplet state can be observed within the fs-TA delay time range, which indicates that the ISC process of DM-Z can take place in a shorter time when dissolved in a non-polar solvent (toluene). According to the excited-state evolution process of fs-TA spectra, the kinetic of ESA peak at 750 nm of fs-TA spectra can be fitted by two exponential functions (Fig. 2d). The detailed data are summarized in Table 2. τ_1 is the CT process to generate S_1(CT). τ_2 is relatively long (about more than 150 ps), this process can be assigned to the vibrational relaxation of S_1(CT). $S_1(CT)_{relax}$ can experience two competing processes: the non-radiative charge recombination (CR) and ISC. Therefore, τ_3 is the lifetime of CR and ISC processes. DM-Z is prone to generate a triplet excited state by the ISC process in DCM solvent, while DM-Z is apt to return to the ground state by the CR process in DMF. Therefore, τ_3 of DM-Z in DCM is longer than that of DMF. According to the theoretical calculation in the next section, DM-Z owns the largest ΔE_{ST}, RISC process is difficult to occur. Thus, τ_4 is ascribed to the non-radiative decay process of the triplet state. By comparing the kinetic of TSCT emitters (DM-B, DM-BX, DM-G, and DM-X), it can be inferred that the TBCT molecule (DM-Z) has a larger ΔE_{ST}, which makes it more difficult to undergo ISC and RISC processes. As a result, the PLQY of DM-Z is the lowest. Hence, the novel TSCT manner is the most feasible strategy for constructing high-performing TADF emitters.

In order to have a deeper understanding of the relationship between the electronic structure of TSCT/TBCT molecules and their luminescent efficiency, the distributions of holes and electrons, IRI analysis, and CT matrix analysis were performed by theoretical calculation [48]. M062X is selected as the function, and Def2-SVP is selected as the bases set to optimize the structures and analyze the distributions of holes and electrons, IRI analysis, and CT matrix of the excited states. Based on the optimized S_1 structures, the adiabatic energy of excited states and spin-orbit coupling (SOC) constant were calculated using ORCA packages. Similar to other D-A emitters, the HOMO is mainly localized on the TPA donor unit, and the LUMO is localized on the triazine acceptor moiety for molecules DM-B, DM-BX, DM-G and DM-X. Whereas for DM-Z, the LUMO is delocalized on the phenyl ring spacer and triazine (Fig. S22 in Supporting information). Meanwhile, in both TSCT and TBCT emitters, the electron- and hole-density patterns of S_1 are localized on the TPA donor and triazine acceptor unit, respectively. These results suggest that the TSCT between donor and acceptor can take place directly in DM-B, DM-BX, DM-G, and DM-X, while for DM-Z, the CT between donor and acceptor is through the bond. C_{hole} and C_{ele}, as two ellipses, are visualized as the isosurface of the hole and electron, respectively. The Δr index is the distance between the centers of C_{hole} and C_{ele}, which can significantly represent the degree of CT [49,50]. As shown in Fig. S22, since the distance between the donor and acceptor of DM-Z is the farthest, its Δr value is the largest, up to 6.133 Å, which means that DM-Z requires more time to reach the CT state, and this result is consistent with the larger τ_1 measured by fs-TA spectra (Tables 1 and 2). Followed by the DM-B and DM-BX, its Δr values are up to 4.469 Å and 4.215 Å, respectively. And the Δr values DM-G and DM-X are 3.338 Å and 3.367 Å, respectively. This indicates that the degree of CT of DM-B

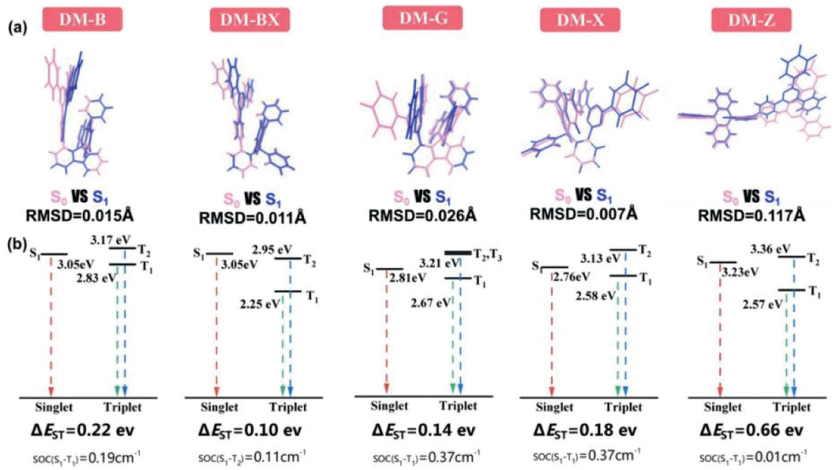

Fig. 3. (a) Geometry comparison and RMSD values between S_0 and S_1. (b) Adiabatic energy landscapes of DM-B, DM-BX, DM-G, DM-X, and DM-Z, respectively.

and DM-BX is greater than DM-G and DM-X, which is consistent with the result of PL spectra and fs-TRUCF spectroscopy that DM-B has a larger spectral redshift. Therefore, τ_1 of DM-B is the largest among the TSCT molecules.

Then the root of the mean of the squared displacement (RMSD) between the optimized structures of S_0 and S_1 was employed to quantitatively analyze the geometric changes for both TSCT and TBCT emitters [51]. The results show that the RMSD value of DM-Z is the greatest up to 0.117 Å, demonstrating that the geometric changes from S_0 to S_1 are the most significant (Fig. 3a). Hence DM-Z needs to spend more time undergoing a structural relaxation process than other emitters, which is consistent with the result of the kinetics of the excited state, where DM-Z has the longest τ_2, reaching 155 ps (dissolved in DCM). Meanwhile, the RMSD value of DM-G (0.026 Å) is larger than other TSCT emitters (the RMSD values of DM-B, DM-BX, and DM-X are 0.015 Å, 0.011 Å, and 0.007 Å, respectively), resulting in DM-G taking more time in structural relaxation process (τ_2 is 19.4 ps in DCM solvent). In addition, the adiabatic energy map can be drawn according to the optimized geometric structure of the singlet and triplet excited states, and the spin-orbit coupling constant (SOC) can be calculated based on the optimized S_1. As shown in Fig. 3b, in DM-Z, the ΔE_{ST} (0.66 eV) is the largest, and the SOC constant (0.01 cm^{-1}) between S_1 and T_1 is quite small, indicating that both ISC and RISC processes are hard to occur for DM-Z. This result further confirms the excited state process of DM-Z obtained by fs-TA. In other emitters, ΔE_{ST} (0.22 eV for DM-B, 0.10 eV for DM-BX, 0.14 eV for DM-G and 0.18 eV for DM-X) is small enough to achieve the ISC conversion from singlet to triplet excited states. The SOC constants of DM-G and DM-X (both 0.37 cm^{-1}) are larger than those of DM-B (0.19 cm^{-1}) and DM-BX (0.11 cm^{-1}). Therefore, DM-G and DM-X are expected to be more likely to undergo ISC than DM-B and DM-BX, which is consistent with the lifetimes of ISC process for DM-G and DM-X getting shorter (τ_3 of DM-G and DM-X are 53.6 ps and 91.9 ps, respectively) than that of DM-B and DM-BX, respectively. Since ΔE_{ST} and SOC values of the TSCT molecules satisfy the prerequisite requirement for ISC and RISC, these molecules are supposed to exhibit a similar RISC and PLQY behavior. In fact, the PLQY of DM-G and DM-X is lower than that of DM-B and DM-BX, suggesting that a particularly critical role except for ΔE_{ST} and SOC probably determines the RISC process in the luminescent performance of TSCT molecules. Besides the ΔE_{ST} and SOC, other factors should also affect the kinetic differences of their RISC process.

Going back to the geometry structures of these molecules, a phenyl ring links the triazine of the acceptor group to the fluorene bridge in DM-B and DM-BX, whereas the triazine is directly linked to the fluorene bridge in DM-G and DM-X. Obviously, it can be speculated that this benzene ring may affect the RISC process. Since IRI can clearly reveal both chemical bond regions and weak interaction regions of donor and acceptor by its isosurfaces [52,53]. As shown in Fig. S23 (Supporting information), the sign(λ_2)ρ values for DM-B, DM-BX, DM-G and DM-X are obviously smaller than that of DM-Z, revealing that the π-π interactions of DM-B, DM-BX, DM-G and DM-X are stronger than that of DM-Z. For DM-B and DM-BX, the π-π stacking interaction is equably concentrated at the gap between the nitrogen-containing six-ring (donor center) and the acceptor moieties in the singlet and triplet excited state, this can boost the TSCT and the reversal of electron spin. For DM-G and DM-X, the dihedral angle between the best-fit planes of the donor and acceptor is very large. Thus the π-π stacking interaction is mainly distributed in the gap near the acceptor side rather than evenly distributed in the gap between the donor center and acceptor. This is not conducive to the TSCT and the reversal of electron spin. Therefore, the degree of electronic communication between donor and acceptor moieties is different among DM-B, DM-BX, and DM-G, DM-X.

To further prove the above conjecture, we used Multiwfn to plot the CT matrix (CTM) and draw heat maps. The CTM is often a good way to reveal actual CT characteristics, and the CTM heat map can provide detailed information about the electronic communication between atoms or fragments. As shown in Fig. 4, we divided DM-B, DM-BX, and DM-Z into seven fragments, and accordingly divided DM-G and DM-X into six fragments, and then drew fragment-fragment CTM and their heat maps in both singlet and triplet excited states. In the S_1, the distance between donor and acceptor moieties in the TBCT molecule (DM-Z) is very far, the frag.2 (donor center) increases electron transfer to frag.1 (fluorene bridge), followed by the frag.7 (benzene ring spacer) and frag.4 (triazine, the center of the acceptor unit). It is worth noting that there is no obvious electronic communication between the benzene ring spacer (frag.7) and triazine (frag.4) in DM-Z. In the DM-B and DM-BX, containing benzene ring spacer, the donor center (frag.2) mainly transfers electrons to the triazine (frag.4) in the S_1, followed by the benzene ring spacer (frag.7). In IRI analysis, there is a strong π-π interaction between the benzene ring spacer and the nitrogen-containing six-ring (center of the donor). Therefore, the donor center (frag.2) can easily transfer electrons to the benzene ring spacer (frag.7) in the S_1. Interestingly, unlike DM-Z, the benzene ring spacer (frag.7) acts as an electron transfer driver to transfer electrons to the triazine (frag.4) in DM-B and

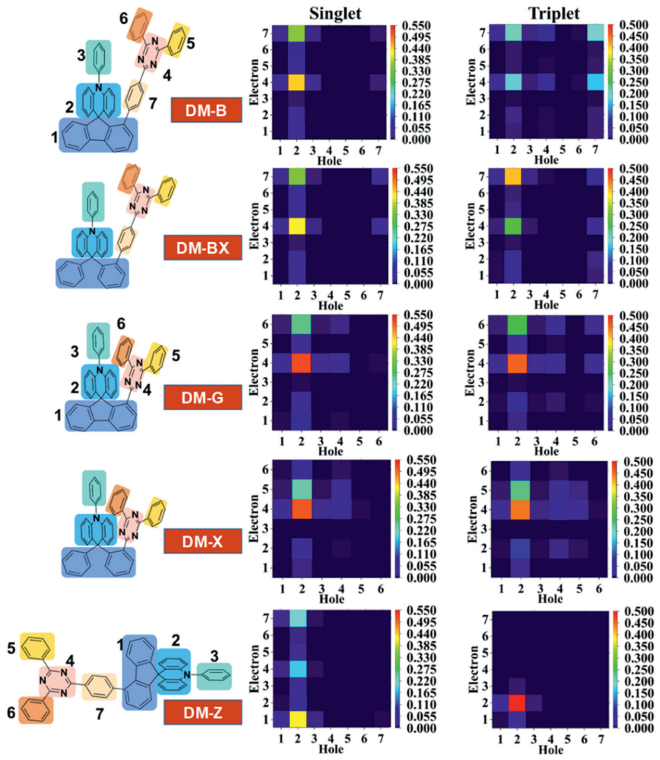

Fig. 4. Calculated the heat map of CT matrix (CTM) analysis. (The amount of electron transfer between fragments is shown in different colors, with red indicating more CT between fragments and purple indicating less).

DM-BX. Therefore, although the distance between the donor center and triazine is relatively large, electron communication can still be achieved between each other, and triazine still maintains its strong electron-absorbing property. In the DM-G and DM-X, similar to DM-B and DM-BX, the donor center (frag.2) mainly transfers electrons to triazine (frag.4) in the S_1, followed by frag.6 (for DM-G) and frag.5 (for DM-X). The difference is that the phenyl ring spacer (frag.7) and acceptor center triazine (frag.4) in DM-G and DM-X will not transfer electrons to frag.6(for DM-G) and frag5 (for DM-X), so the degree of CT is further reduced.

However, the triplet state of DM-Z is mainly local excitation. There is no electron transfer between the donor center (frag.2) and triazine (frag.4). For DM-B, there is an electronic communication between triazine (frag.4) and benzene ring spacer (frag.7) in the triplet state, and benzene ring spacer (frag.7) still acts as an electron transfer driver, transferring more electrons to triazine (frag.4). Especially, the donor center (frag.2) mainly transfers electrons to the benzene ring spacer (frag.7) for DM-BX, followed by triazine (frag.4). According to IRI analysis, the reasons may be that the triazine (frag.4) and donor center (frag.2) do not have a good face-to-face arrangement in the triplet excited state like S_1. Nevertheless, frag.7 still acts as an electron transfer driver to promote transferring more electrons to triazine (frag.4) in the triplet state, maintaining the strong electron acceptor property of triazine. Like S_1, the triazine (frag.4) transfers electrons to frag.6 (for DM-G) and frag.5 (for DM-X) in the triplet state, respectively, while frag.6 (for DM-G) and frag.5 (for DM-X) transfer only a small number of electrons back to frag.4 (very dark in the heat map). As a result, the efficient RISC process and then high PLQY can be achieved for DM-B and DM-BX with a benzene ring spacer [54].

TADF emitters are usually taken as the aggregated state to prepare OLED devices. Therefore, it is necessary to explore the excited state evolution process and luminescent mechanism of TADF materials in thin film. The steady-state spectra results indicate that the UV–Vis absorption spectra of TSCT molecules (DM-B, DM-BX, DM-G and DM-X) in thin film (the doping ratio is 4 wt%, doped in polymethyl methacrylate (PMMA)) are similar to that in the solution phase (Figs. S24 and S25 in Supporting information). However, the emission peaks of films for these emitters display some degree of blue shift, indicating that the molecular vibrations are inhibited in the solid phase. According to the results of PL, DM-BX exhibits the highest PLQY, reaching 67.4%, followed by DM-B (53.9%), DM-G (39.4%) and DM-X (11%) (Fig. S26 in Supporting information). However, DM-B exhibits the highest PLQY of 56.1%, followed by DM-BX (45.4%) in DCM solvent. A difference between these can be attributable to the limitation of molecular rotations and vibrations in the film for DM-BX, which is conducive to the improvement of PLQY. In order to unveil the reason for affecting PLQY from the perspective of excited state dynamics, fs-TA and ns-TA spectra experiments were performed on the film of four TSCT molecules. Fig. S27a (Supporting information) demonstrates that the fs-TA spectra of DM-B display three spectral change processes. At the beginning of 0.37 ps, the ESA peak at 658 nm rises quickly. After that, the ESA peak at 750 nm (the characteristic peak of TPA cation radical) slightly rises, thus this process can be attributed to the CT process that generates an excited CT state. Finally, the ESA peak at 435 nm gradually rises, which may be assigned to ISC, converting ^{1}CT into T_1. To trace the whole excited state evolution process of DM-B, ns-TA experiments were performed on the film of DM-B. As shown in Fig. S27b (Supporting information), the ESA peaks at 415 nm and 670 nm quickly rise, and then decays to zero at about 11 μs. The kinetic comparison of these two ESA peaks indicates that they have similar kinetic decay processes (Fig. S27c in Supporting information), revealing that these two ESA peaks come from the same excited state species. Meantime, the ESA peaks at 415 nm and 670 nm are similar to that of ns-TA for DM-B in DCM. Therefore, these two ESA peaks are assigned to the triplet excited state of DM-B. In addition, the films of DM-BX, DM-G, and DM-X were also explored by fs-TA and ns-TA spectra. The results illustrate that all of them have similar excited-state evolution processes to that of DM-B (Figs. S28-S30 in Supporting information), except for the different lifetimes of the excited-state dynamics. The specific lifetimes of triplet excited states are obtained by two exponential functions fitting on its kinetic decay curve (Fig. S31 in Supporting information). According to the kinetics analysis of these emitters in the solution phase, τ_1 can be assigned to the lifetime of the RISC process of the triplet excited state, and τ_2 is attributed to the relaxation process of the remaining triplet excited state. In detail, τ_1 of DM-BX is 22.5 ns and its weighted amplitude is up to 79.8%, indicating that most of the triplet excited state returns to the singlet excited state through the RISC process, and then emits the delayed fluorescence. For DM-B, although τ_1 has a relatively large weight (66.7%), the RISC process is relatively slow (56 ns), so its PLQY is 53.9%, smaller than that of DM-BX. For DM-G, the weighted amplitude of τ_1 is only 37.3%, which means most of the triplet excited state returns to the ground state through a non-radiative relaxation process, thus PLQY of DM-G is 39.4%. However, for DM-X molecules, the ESA peak at 640 nm dramatically drops, while the ESA peak at short-wavelength for the triplet state does not obviously rise in fs-TA spectra, revealing that the singlet excited state can not convert into the triplet excited state through the ISC process. Possibly, the singlet excited state of DM-X mainly returns to the ground state through non-radiative transition such as molecular vibration, leading to its PLQY being the lowest, which is in line with previous studies [38]. In general, the PLQY of TSCT emitters is determined by both ISC and RISC in the thin film phase.

In conclusion, to explore the photophysical processes and luminescent mechanism of TSCT and TBCT molecules and unveil the factors that affect the PLQY of TADF molecules, four TSCT molecules and one TBCT molecule were investigated by ultrafast fs-TA, ns-TA spectra, and theoretical calculations. The relationship between the geometry and electronic structures and luminescent efficiency was built up *via* tracing excited state evolution processes. Firstly, the large ΔE_{ST} of TBCT molecule DM-Z resulted in a slow ISC process and the absence of the RISC process, being consistent with the quite low PLQY of DM-Z. In contrast, the ISC process can occur in a shorter lifetime for TSCT molecules. Notably, the RISC process is the determining factor affecting the PLQY of TSCT emitters. An efficient RISC process can be realized in DM-B and DM-BX. Significantly, DM-B and DM-BX containing benzene ring spacers exhibit better π-π stacking interaction and have higher PLQY whether it's in a solvent or a film. Importantly, the benzene ring spacer acts as an electron transfer driver, transferring an electron to the center of accepter triazine, and facilitating the electron communication in DM-B and DM-BX, which are better than that of DM-G and DM-X molecules with no benzene spacer, leading to a further improvement in PLQY for DM-B and DM-BX. The introduction of the benzene ring spacer can not only generate efficient face-to-face π-π interaction between donor and acceptor but also improve the degree of charge separation so as to achieve good electronic communication in the CT process, and thus improve the luminescent performance of TADF materials.

It must be noted that DM-BX exhibits the highest PLQY, reaching 67.4%, followed by DM-B (53.9%) in the film state. Ultrafast transient absorption studies on DM-BX and DM-B indicate that most of the triplet excited state returns to the singlet excited state through the RISC process, and then emits the delayed fluorescence. For DM-G, most of the triplet excited state returns to the ground state through a non-radiative relaxation process, thus PLQY value of DM-G is 39.4% in the film state. However, for DM-X, the singlet excited state cannot efficiently convert into the triplet excited state through the ISC process. The singlet excited state of DM-X mainly returns to the ground state through non-radiative transition such as molecular vibration, leading to its PLQY being the lowest. Therefore, the precise excited state dynamics study of TSCT molecules has paved the way for the design of high-performance TADF materials.

Declaration of competing interest

The authors declare no competing financial interest.

CRediT authorship contribution statement

Manlin Lu: Writing – original draft, Methodology, Investigation, Data curation. **Sheng Liao:** Investigation. **Jiayu Li:** Investigation. **Zidong Yu:** Investigation. **Ningjiu Zhao:** Investigation. **Zuoti Xie:** Investigation. **Shunli Chen:** Investigation. **Li Dang:** Writing – review & editing, Investigation. **Ming-De Li:** Writing – review & editing, Project administration, Methodology, Investigation, Funding acquisition, Conceptualization.

Acknowledgments

This project was financially supported by the National Natural Science Foundation of China (No. 22273057), the Universities Joint Laboratory of Guangdong, Hong Kong and Macao (No. 2021LSYS009) and the Natural Science Foundation of Guangdong Province (Nos. 2022A1515011661, 2023A1515012631), the Chemistry and Chemical Engineering Guangdong Laboratory (No. 1922003) and Guangdong Major Project of Basic and Applied Basic Research (No. 2019B030302009).

Supplementary materials

Supplementary material associated with this article can be found, in the online version, at doi:10.1016/j.cclet.2024.110066.

References

[1] H. Uoyama, K. Goushi, K. Shizu, H. Nomura, C. Adachi, Nature 492 (2012) 234–238.
[2] X.Q. Wang, S.Y. Yang, Q.S. Tian, et al., Angew. Chem. Int. Ed. 60 (2021) 5213.
[3] B. Zhou, Z. Qi, M. Dai, C. Xing, D. Yan, Angew. Chem. Int. Ed 62 (2023) e202309913.
[4] B. Zhou, Z.D. Yan, Adv. Funct. Mater. 29 (2019) 1807599.
[5] C. Xing, B. Zhou, D. Yan, W.H. Fang, Adv. Sci. 11 (2024) 2310262.
[6] G. Xiao, Y.J. Ma, Z. Qi, et al., Chem. Sci. 10 (2024) 3625–3632.
[7] M. Saigo, K. Miyata, S.I. Tanaka, et al., J. Phys. Chem. Lett. 10 (2019) 2475–2480.
[8] A. Endo, K. Sato, K. Yoshimura, et al., Appl. Phys. Lett. 98 (2011) 083302.
[9] Y. Yuan, Y. Hu, Y.X. Zhang, et al., Adv. Funct. Mater. 27 (2017) 1700986.
[10] Q. Zhang, H. Kuwabara, W.J. Potscavage, et al., J. Am. Chem. Soc. 136 (2014) 18070–18081.
[11] H. Tsujimoto, D.G. Ha, G. Markopoulos, et al., J. Am. Chem. Soc. 139 (2017) 4894–4900.
[12] S. Shao, J. Hu, X. Wang, et al., J. Am. Chem. Soc. 139 (2017) 17739–17742.
[13] K. Li, Y. Zhu, B. Yao, et al., Chem. Commun. 56 (2020) 5957–5960.
[14] C. Wu, W. Liu, K. Li, et al., Angew. Chem. Int. Ed. 60 (2021) 3994–3998.
[15] A.J. Gillett, A Pershin, R. Pandya, et al., Nat. Mater. 21 (2022) 1150–1157.
[16] S. Kumar, L.G. Franca, K. Stavrou, et al., J. Phys. Chem. Lett. 12 (2021) 2820–2830.
[17] Y.K. Wang, C.C. Huang, H. Ye, et al., Adv. Opt. Mater. 8 (2020) 1901150.
[18] F. Ma, H. Ji, D. Zhang, et al., Dyes Pigm 188 (2021) 109208.
[19] X. Wang, S. Wang, J. Lv, et al., Chem. Sci. 10 (2019) 2915–2923.
[20] C.C. Peng, S.Y. Yang, H.C. Li, et al., Adv. Mater. 32 (2020) 2003885.
[21] B. Li, Z. Yang, W. Gong, et al., Adv Opt. Mater. 9 (2021) 2100180.
[22] M. Auffray, U. Balijapalli, J.C. Ribierre, Y. Tsuchiya, C. Adachi, Chem. Lett. 49 (2020) 932–935.
[23] Y. Song, M. Tian, R. Yu, L. He, ACS Appl. Mater. Interfaces 13 (2021) 60269–60278.
[24] S. Kumar, L.G. Franca, K. Stavrou, et al., J. Phys. Chem. Lett. 12 (2021) 2820–2830.
[25] B. Du, X. Wang, F. Chen, et al., Chem. Commun. 57 (2021) 7144–7147.
[26] J. Hu, Y. Wang, Q. Li, et al., Chem. Sci. 12 (2021) 13083–13091.
[27] J.T. Ye, Y.Q. Qiu, Phys. Chem. Chem. Phys. 23 (2021) 15881–15898.
[28] R. Wang, Z. Li, T. Hu, et al., ACS Appl. Mater. Interfaces 13 (2021) 49066–49075.
[29] T. Huang, Q. Wang, S. Xiao, et al., Angew. Chem. 133 (2021) 23964–23969.
[30] S. Shao, L. Wang, X. Jing, F. Wang, Angew. Chem. Int. Ed. 60 (2021) 16585–16593.
[31] T. Huang, Q. Wang, G. Meng, L. Duan, D. Zhang, Angew. Chem. 134 (2022) e202200059.
[32] Z. Zhao, C. Zeng, X. Peng, et al., Angew. Chem. Int. Ed. 61 (2022) e202210864.
[33] F.M. Xie, H.Z. Li, K. Zhang, et al., Angew. Chem. Int. Ed. 61 (2022) e202213823.
[34] C. Jiang, J. Miao, D. Zhang, et al., Research 2022 (2022) 9892802.
[35] A. Ruduss, B. Turovska, S. Belyakov, et al., Inorg. Chem. 61 (2022) 2174–2185.
[36] S.Y. Yang, Z.Q. Feng, Z. Fu, et al., Angew. Chem. 134 (2022) e202206861.
[37] Y. Zhang, S.L. Lai, Q.X. Tong, et al., Chem. Mater. 24 (2012) 61–70.
[38] X. Tang, L.S. Cui, H.C. Li, et al., Nat. Mater. 19 (2020) 1332–1338.
[39] H. Zou, H. Liu, Q. Mu, et al., Spectrochim. Acta Part A 285 (2023) 121899.
[40] M.D. Li, N.K. Wong, J. Xiao, et al., J. Am. Chem. Soc. 140 (2018) 15957–15968.
[41] Z. Deng, S. Sun, M. Zhou, et al., J. Phys. Chem. Lett. 10 (2019) 6499–6503.
[42] S. Yang, C. Cao, J. Li, et al., J. Phys. Chem. C 126 (2022) 1076–1084.
[43] M.J. Frisch, G.W. Trucks, H.B. Schlegel, et al., Gaussian 16, Revision C.01, Gaussian, Inc., Wallingford, CT, 2016.
[44] A.P. Kulkarni, S.A. Jenekhe, J. Phys. Chem. C 112 (2008) 5174–5184.
[45] M. Uebe, T. Kazama, R. Kurata, D. Sakamak, A. Ito, Angew. Chem. Int. Ed. 56 (2017) 15712–15717.
[46] J.A. Lin, S.W. Li, Z.Y. Liu, et al., Chem. Mater. 31 (2019) 5981–5992.
[47] Z. Wang, X. Gou, Q. Shi, et al., Angew. Chem. 134 (2022) e202207619.
[48] T. Lu, F.J. Chen, Comput. Chem. 33 (2012) 580–592.
[49] S. Yang, C. Cao, J. Li, et al., Chem. Eur. J. 27 (2021) 1337–1345.
[50] Z. Liu, T. Lu, Q. Chen, Carbon 165 (2020) 461–467.
[51] H. Zou, Y. Ma, H. Liu, et al., J. Mater. Chem. C 10 (2022) 517–531.
[52] T. Lu, Q. Chen, Chem. Methods 1 (2021) 231–239.
[53] G. Cai, Z. Chen, X. Xia, et al., Adv. Sci. 9 (2022) 2200578.
[54] C. Zhou, Y. Liu, Z. Sun, et al., Dyes Pigm. 205 (2022) 110488.